The early Upper Paleolithic site Crvenka-At, Serbia: the first Aurignacian lowland occupation site in the Southern Carpathian Basin

Nett, J.J.; Chu, W.; Fischer, P.; Hambach, U.; Klasen, N.; Zeeden, C.; ... ; Lehmkuhl, F.

frontiers in Earth Science

ORIGINAL RESEARCH
published: 26 February 2021
doi: 10.3389/feart.2021.599986

The Early Upper Paleolithic Site Crvenka-At, Serbia–The First Aurignacian Lowland Occupation Site in the Southern Carpathian Basin

Janina J. Nett[1], Wei Chu[2], Peter Fischer[3], Ulrich Hambach[4], Nicole Klasen[5], Christian Zeeden[1,6], Igor Obreht[1,7], Lea Obrocki[3], Stephan Pötter[1], Milivoj B. Gavrilov[8], Andreas Vött[3], Dušan Mihailović[9], Slobodan B. Marković[8] and Frank Lehmkuhl[1]*

[1]Department of Geography, Physical Geography and Geoecology, RWTH Aachen University, Aachen, Germany, [2]Institute of Prehistoric Archeology, University of Cologne, Cologne, Germany, [3]Institute for Geography, Natural Hazard Research and Geoarchaeology, Mainz, Germany, [4]BayCEER & Chair of Geomorphology, University of Bayreuth, Bayreuth, Germany, [5]Cologne Luminescence Laboratory, Institute of Geography, University of Cologne, Cologne, Germany, [6]Department of Rock Physics and Borehole Geophysics, Leibniz Institute for Applied Geophysics, Hannover, Germany, [7]Organic Geochemistry Group, MARUM-Center for Marine Environmental Sciences and Department of Geosciences, University of Bremen, Bremen, Germany, [8]Chair for Physical Geography, Faculty of Science, University of Novi Sad, Novi Sad, Serbia, [9]Department of Archeology, Faculty of Philosophy, University of Belgrade, Belgrade, Serbia

OPEN ACCESS

Edited by:
David K. Wright,
University of Oslo, Norway

Reviewed by:
Kaja Fenn,
University of Oxford, United Kingdom
Theodoros Karampaglidis,
Research Centre and Museum for Human Behavioural Evolution, Germany

***Correspondence:**
Janina J. Nett
Janina.boesken@geo.rwth-aachen.de

Specialty section:
This article was submitted to Quaternary Science, Geomorphology and Palaeoenvironment, a section of the journal Frontiers in Earth Science

Received: 28 August 2020
Accepted: 21 January 2021
Published: 26 February 2021

Citation:
Nett JJ, Chu W, Fischer P, Hambach U, Klasen N, Zeeden C, Obreht I, Obrocki L, Pötter S, Gavrilov MB, Vött A, Mihailović D, Marković SB and Lehmkuhl F (2021) The Early Upper Paleolithic Site Crvenka-At, Serbia–The First Aurignacian Lowland Occupation Site in the Southern Carpathian Basin. Front. Earth Sci. 9:599986. doi: 10.3389/feart.2021.599986

The Carpathian Basin is a key region for understanding modern human expansion into western Eurasia during the Late Pleistocene because of numerous early hominid fossil find spots. However, the corresponding archeological record remains less understood due to a paucity of well dated, contextualized sites. To help rectify this, we excavated and sampled Crvenka-At (Serbia), one of the largest Upper Paleolithic sites in the region to obtain radiometric ages for the archeological artifacts and evaluate their depositional context and subsequent site formation processes. Our results confirm that this locality represents a multiple-occupation Aurignacian site that dates to 36.4 ± 2.8 ka based on modeling of luminescence ages. Electrical resistivity tomography measurements indicate that the site formed on a sandy-gravelly fill terrace covered by overbank deposits. Complex grain size distributions further suggest site formation in contrasting depositional environments typically occurring alongside fluvial channels, at lakeshores, in alluvial fan or delta settings. The site is thus the closest (ca. 50 km) known Aurignacian site to the earliest undisputed modern human remains in Europe at the Peştera cu oase and some intervals of the occupation may therefore have been contemporaneous with them. This suggests that modern humans, during their initial settlement of Europe, exploited a wider range of topographic and ecological settings than previously posited. Our findings indicate that lowland areas of the Carpathian Basin are an important part of understanding the early settlement patterns of modern humans in Europe.

Keywords: late pleistocene, MIS 3, middle danube basin, luminescence dating, aurignacian, paleoenvironment, modern human, banat

INTRODUCTION

While it is generally accepted that the initial dispersal of modern humans into western Eurasia originated in Africa, the timing, trajectory and conditions of this spread are still not fully understood (e.g., Davies et al., 2015; Obreht et al., 2017; Staubwasser et al., 2018; Teyssandier and Zilhão, 2018; Bösken, 2020; Hublin et al., 2020). An often-discussed potential trajectory of human migration into Central Europe is along the Danube, where river valleys and/or piedmonts have been suggested as possible ecological corridors (Kozłowski, 1992; Zilhão et al., 2007; Conard and Bolus, 2008; Hauck et al., 2018; Chu, 2018). Central to this discussion is the Banat, a geographically and environmentally diverse region in the southeastern Carpathian Basin shared by Romania, Serbia and Hungary. This region holds a key geographical position immediately northwest of the Iron Gates, the only hydrological connection between Central and Southeastern European continental drainage systems (Schwarz, 2014; Krézsek and Olariu, 2020).

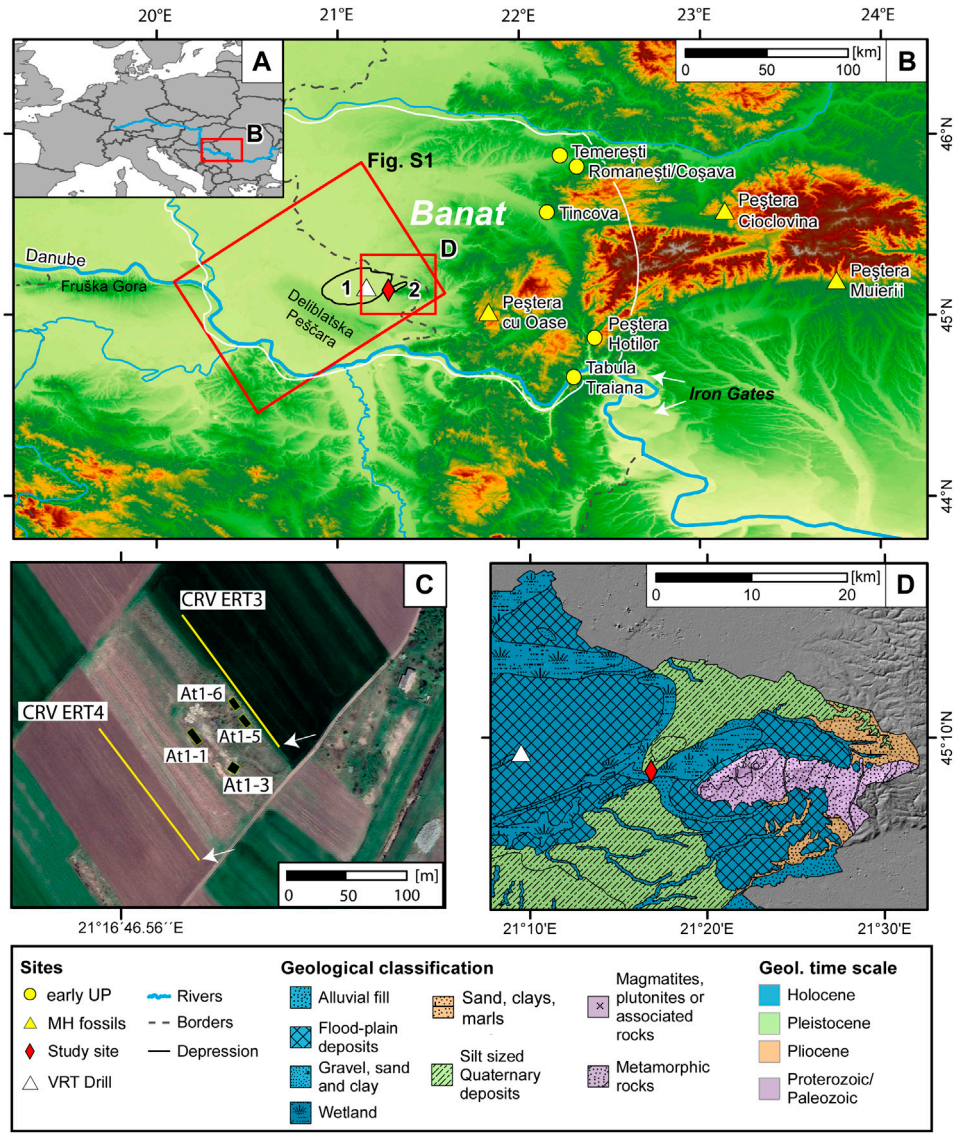

FIGURE 1 | Location **(A–C)** and geology **(D)** of the research site Crvenka-At (red diamond) east of the Deliblatska Peščara dune field and the Alibunar Depression (1) and west of the Vršac Mountains (2; map **B)**. The site is located at the border to two morphological depressions (black lines). Several sites that contain early Upper Palaeolithic artifacts are indicated (yellow circles). Caves containing early modern human remains are marked with yellow triangles. Furthermore, the location of the Vršac borehole is shown (white triangle; Zeeden et al., 2021). The ALOS Global Digital Surface Model (AW3D30) builds the basemap for the surface elevation ©JAXA (JAXA EORC, 2016). The extend of **Figure S1** is indicated (red rectangle). The Banat region is located within the white lines. Map **(C)** shows a close-up of the At I site including the ERT transects and the excavation trenches. The arrows indicate electrodes 48 of each transect. The google base map (Bilder © 2020 CNES/Airbus, Maxar Technologies, Kartendaten ©) shows a satellite photo. The geological map in D uses the map provided by the Geological Institute of Serbia, 2009.

Archeological interest in the Banat area increased after the discovery of early modern human remains at the Peștera cu oase (ca. 42–37 ka cal BP; Trinkaus et al., 2003a; Trinkaus et al., 2003b; Trinkaus et al., 2012). The conspicuous absence of accompanying archeological artifacts stimulated the re-investigation of the open-air sites of Românești, Coşava and Tincova (**Figure 1**) that highlight the archeological importance of the Banat during the early Upper Paleolithic (e.g., Anghelinu et al., 2012; Sitlivy et al., 2012; Kels et al., 2014; Sitlivy et al., 2014; Chu et al., 2016b). Furthermore, abundant, nearby loess archives have augmented our understanding of the prevailing palaeoenvironmental conditions during the Late Pleistocene (e.g., Schmidt et al., 2013; Kels et al., 2014; Schulte et al., 2014; Obreht et al., 2015; Zeeden et al., 2016; Gavrilov et al., 2018; Pötter et al., 2020).

Many open-air archeological sites from the early Upper Paleolithic in the Banat (and many sites within the wider Carpathian Basin) have been recovered in an approximate altitudinal belt of 200–300 m above mean sea level (AMSL; Hauck et al., 2018) where artifacts have been mainly excavated in pedogenic complexes that developed in the Carpathian foothills during Marine Isotope Stage (MIS) 3 (Kels et al., 2014). Research has thus far focused on archeological sites along the western foothills of the Carpathian Mountains. However, those sites are characterized by short sections (<3 m) of Upper Pleistocene sediments thereby hindering high-resolution dating and palaeoenvironmental analyses (e.g., Kels et al., 2014; Chu et al., 2016b; Chu et al., 2019). On the other hand, other geomorphological settings (e.g., lower altitudes) of the Carpathian Basin have received little attention, thereby limiting a broader understanding of how modern humans interacted with the landscape (Dobos and Chu, 2019). This may be related to either a true absence of archeological sites, problematic sedimentological archives with high deposition rates that obscure archeological findings (Tourloukis, 2016) or limited systematic research (Fitzsimmons et al., 2012; Iovita et al., 2014; Chu et al., 2016b; Mihailović, 2020).

To examine the latter possibility, a re-excavation campaign was undertaken at Crvenka-At in the vicinity of Vršac, in northern Serbia, between 2014 and 2015. The site was chosen for proximity to the Peștera cu oase, its unique topographic position and its well attributed stratified Aurignacian assemblages that remained undated by absolute dating methods. The aim of the study was to extend our knowledge of early modern human occupation in the lowland areas of the Carpathian Basin by investigating its timing and environmental context.

BACKGROUND

Research Site and Site History

Crvenka-At (45°08.104′ N, 21°16.853′ E) is an archeological site complex comprising at least two separate localities (Crvenka and At) and other find spots located approximately 3 km north of the town of Vršac (northeastern Serbia) in the southeastern part of the Carpathian Basin (**Figure 1**). Both localities are situated within a ridge (top ~93 m AMSL; At I ~87 m AMSL; At II ~86 m AMSL; bottom of depressions ~76–82 m AMSL) separating depressions north of Vršac and east of Alibunar The Alibunar Depression (**Figure 1B**) was described as a *morass* (i.e., mire/mud/swamp) in the map of 1769 but was later drained at the turn of the 18th century (Müller, 1769; Timár et al., 2008). The depression is bounded by the Deliblatska/Banatska Peščara loess and dune fields to the west and the Vršac Mountains to the east. Middle and Upper Paleolithic artifacts from the northern foothills of the Vršac Mountains were first discovered during sand extraction in the 19th century. More systematic collection at the Crvenka-At sites was undertaken by R. Rašajski (1952–1978) that highlighted the technological homogeneity of the recovered artifacts (Mihailović et al., 2011). A test excavation in 1984 identified three separate archeological levels containing 19 flints and several dozen quartz artifacts (Radovanović, 1986). These were later attributed to "typical" Aurignacian (IIa at At and IIb at Crvenka) and "Krems" style Aurignacian assemblages (Layer IIb at Crvenka; Mihailović, 1992) based on their typological characteristics. Against this background, the site was relocated through a series of trench excavations and its sedimentary and environmental contexts were investigated through chronostratigraphical dating and sedimentological analyses (cf. Chu et al., 2014; Chu et al., 2016a).

Geological and Geomorphological Setting

The area of the Vršac Mountains is part of the southeastern margin of the Carpathian Basin that tectonically formed during the Neogene and Quaternary periods (Matenco and Radivojević, 2012; Sušić et al., 2016; Bartha et al., 2018; Rundić et al., 2019). The present-day landscape in the Carpathian Basin is also strongly affected by neo-tectonic processes, with the youngest tectonic deformations characterized by positive and negative vertical motions (Toljić et al., 2013). The central and southeastern part of the basin, where the research area is located, is dominated by northeast-southwest and northwest-southeast oriented strike-slip faults (Marović et al., 2007; Sušić et al., 2016). This tectonic regime resulted beside rapidly uplifting blocks (e.g., Vršac Mtns.) in the development of the Alibunar Depression (**Figure 1**), which was filled with fluvial sediments as it is connected to a river system, something that is typical for such structural depressions. The geological map in **Figure 1D** depicts the ridges as Pleistocene silts (green) and the basins as Holocene wetland and floodplain deposits (blue). This underlines the ongoing subsidence of the basin. The Vršac Mountains as push-up structure contain crystalline basement rocks of Paleoproterozoic–Paleozoic age (purple) covered by Pliocene marls, sands and silts (orange). Further information on the dynamic landscape evolution can be found in the Supplementary Material (cf. **Supplementary Figure S1**).

MATERIALS AND METHODS

Excavation and Sampling

In 2015, eight test trenches were prepared at the edge of two pre-existing sand extraction pits (At I and At II). The first trench was

excavated to locate the 1984 excavation trench by Radovanović (At II). Seven other trenches were excavated at the margins of an adjacent sand pit (At I) to clarify the sedimentary setting and to correlate the stratigraphy of At I and At II with the Crvenka locality (see Chu et al., 2014; Chu et al., 2016a). Here, we focus on two of these trenches: trench 3 and 5. All finds and the excavation areas were piece-provenienced in a local coordinate system using both traditional analogue methods and a total station.

Eight luminescence samples and corresponding radionuclide concentration samples were extracted at two trench profiles (At I-3B and At I-5) with the highest artifact density in order to chronostratigraphically constrain the archeological levels. In addition, sediment samples were collected for grain size analyses and color measurements in 2 cm intervals to investigate the palaeoenvironmental setting of the site. **Supplementary Figure S2** shows photographs of the sampled profiles.

Electrical Resistivity Tomography

Electrical resistivity tomography (ERT) was conducted to detect stratigraphic differences within the near-surface deposits and to map the underlying bedrock topography. A Syscal R1+ Switch 48 device (Iris Instruments) and a Wenner-Schlumberger electrode array with 3 m electrode spacing were used allowing for an investigation depth of approximately 18 m below surface. The elevation and geographical position of each electrode were measured using a differential GPS (type Topcon HiPerPRO). GPS altitudes were corrected to m AMSL based on known altitudes from topographical fixed points at the excavation site. Data were then inverted incorporating the topography using the Res2Dinv inversion program (Geotomo Software).

Optically Stimulated Luminescence Dating of Sediments

Samples were separated into 100–150 and 150–200 µm fractions. Only for sample C-L4241, grain sizes between 100 and 250 µm were used due to a low amount of sample material. Both quartz and potassium feldspar grains were extracted. Further sample preparation and measurement facilities are described in detail in the **Supplementary Material**. A single aliquot regenerative dose (SAR) protocol (Murray and Wintle, 2000; Murray and Wintle, 2003) was applied for quartz. A preheat plateau test (Murray and Wintle, 2000) and a dose recovery test (DRT, e.g., Murray and Wintle, 2003) were performed on sample C-L4240 before D_e (equivalent dose) measurements to assess the proper measurement settings.

For potassium feldspar measurements, post-infrared infrared stimulated luminescence ($pIRIR_{290}$ and $pIRIR_{225}$) protocols were tested (Buylaert et al., 2009; Thiel et al., 2011). Prior infrared (IR) stimulation temperature tests were performed (Buylaert et al., 2012). Furthermore, DRTs using bleached samples (24 h Hönle Sol2 solar simulator) were conducted. These tests were carried out on samples C-L4239–C-L4242. Finally, the equivalent dose was determined on a minimum of 28 aliquots per sample using an arithmetic mean. Residual doses were assessed after bleaching the aliquots for 24 h in a solar simulator. Fading tests were conducted on sample C-L4240 using three aliquots per tested protocol and pause times of 6,000, 12,000, 24,000, and 48,000 s.

For the determination of dose rates, radionuclide concentrations were measured on a high-purity germanium gamma-ray spectrometer. Additionally, the saturation water content of one sample representative for the sand layer (unit C in **Figure 2**) was determined by centrifuging and adding water until the sediment reached its maximum absorption capacity (following the example of Nelson and Rittenour, 2015). The dose rates and ages were calculated using the Adele software (Kulig, 2005).

The luminescence dating results were further analyzed using the Bayesian ADMin model (Zeeden et al., 2018) to build an age-depth model. The model runs in the R environment (R Core Team, 2020). The corresponding R script can be found in the **Supplementary Material** (Section 4). Prior to modeling, the pIR ages of both profiles were combined by transferring the depths of samples in trench 3B into the depth scale of trench 5.

Grain Size Analysis

All grain size samples were prepared following the methods described in Nottebaum et al. (2015) and Schulte et al. (2016). Grain size was measured with a Laser Diffraction Particle Size Analyzer (Beckman Coulter LS 13 320) calculating the percentaged size frequency of 116 classes within a size range of 0.04–2,000.00 µm (2% uncertainty). The measurement accuracy was increased by measuring each sample four times in two different concentrations. The grain size distributions were determined using the Mie theory (ISO, 2009; Fluid RI: 1.33; Sample RI: 1.55; Imaginary RI: 0.1; Özer et al., 2010; cf.; Schulte et al., 2016).

Spectrophotometric Analysis

The colorimetric properties of the sediments were determined as described in e.g., Eckmeier et al. (2013) and Vlaminck et al. (2016) using a Konica Minolta CM-5 spectrophotometer after the samples were homogenized and dried. The L*a*b* values indicate the extinction of light, on a scale from L* 0 (absolute black) to L* 100 (absolute white) and express color as chromaticity coordinates on red-green (a*) and blue-yellow (b*) scales. Measured colors were plotted in *R* using the 'drawProfile.R' script (Sprafke, 2016; Zeeden et al., 2017).

RESULTS

Stratigraphy

The stratigraphic succession of At I trench 5 started with fine white sands showing a fining up trend as coarser sands and mica flitters occur at the profile base (4.45–4.20 m depth; see **Figure 2**; **Supplementary Figure S2**; description follows ISO 11277, 2009). At a depth of 4.20 m, some organic material was present, potentially from rootlets. On top of this, layered orange, beige, and white sands with fine gravels with diameters up to 4 mm accumulated (4.20–4.06 m). Above, from 4.06 to 3.95 m, beige sands with occasional fine gravels (within the sandy matrix) were deposited. These were overlain by a homogeneous bed of beige

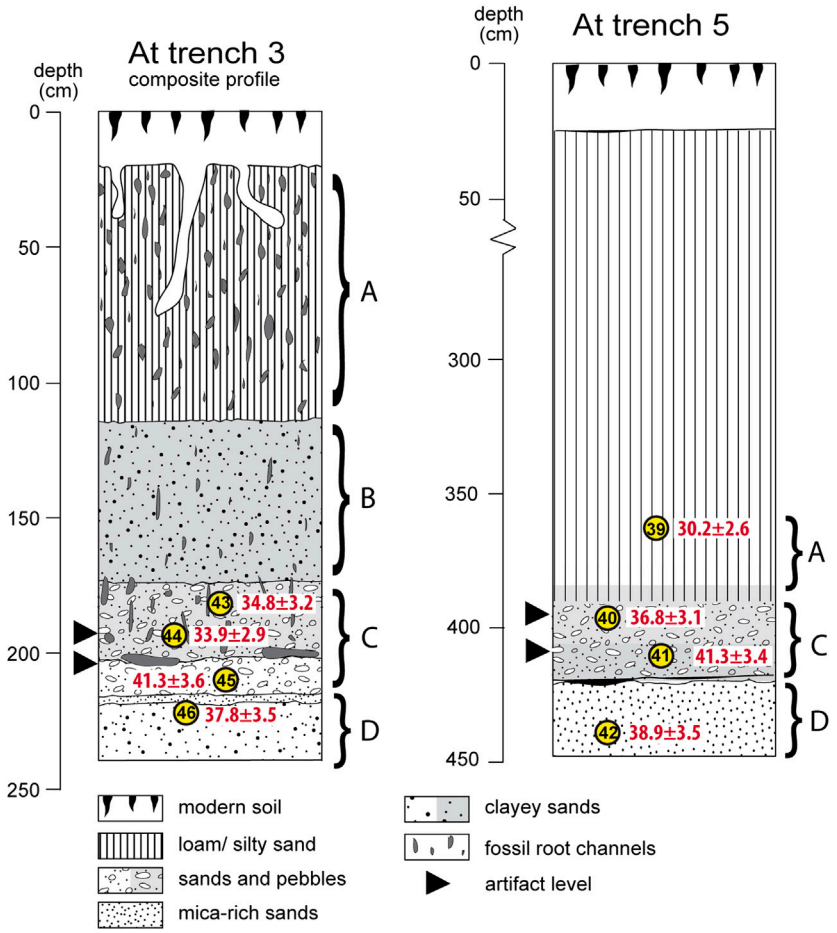

FIGURE 2 | Profile sketches show a composite of At trench 3A and 3B on the left and trench 5 on the right. The artifact find levels are shown with black triangles. For trench 3 these include the faunal remains. Location of luminescence samples are illustrated and labeled with the last two digits of the laboratory numbers in yellow circles. Luminescence ages are shown in red next to these. Letters A–D indicate the different units as used in **Figure 7**.

silty sands (3.95–3.85 m). At a depth of 3.85 m, dark brown organic material with bedding-parallel orientation was present. The horizon from 3.85 to 3.60 m consisted of dark brown sands and silts that fined upwards. Numerous rootlets were also present. The upper ~3.60 m of the profile belonged to the same stratigraphic unit as the dark brown silts, but were not investigated in detail. **Figure 2** shows the stratigraphical column of the section.

In trench 3, two profiles were investigated (cf. **Figure 2**; **Supplementary Figure S2**). Their stratigraphy was similar to trench 5, but contained rootlet channels throughout the profiles. A composite profile for trench 3 was made using both profile descriptions and the grain size data for correlation (**Figure 2**). The profile descriptions of the sub-profiles is found in the **Supplementary Material**. The composite profile At I-3 has a depth of 2.40 m. The sequence started with a layer of mica-bearing (loamy) sands (2.20–2.40 m), followed by mica-rich golden sands (2.17–2.20 m). Above, a clast-supported layer of white sands and fine gravels accumulated (2.03–2.17 m). This was overlain by a matrix-supported ash-gray (reductimorphic) bed of intercalated coarse sands and very fine gravels (1.74–2.03 m) that contained humic rootlet channels and was overlain by matrix-supported clayey sands with orange mottles (redoximorphic features; 1.15–1.74 m). The upper part of the sequence was characterized by an ochre-gray, bioturbated and inhomogeneous bed of sandy loam (0.15–1.15 m) containing occasional fine gravels. The top unit comprised the recent brown humic soil (0.15 m to the top). Approximately 1.6 m of sediment was missing on top due to agricultural activities (deduced from the maximum height measured at the outcrop using the total station).

Excavation

Trenches installed at the margins of the sandpits preserved deposits dating to the Neolithic Vinča (ca. 5500–4500 BCE) and Starčevo (ca. 6200 BCE and 5500 BCE) cultures (Chapman, 2000, 237–239; Chu et al., 2016a), followed by sterile sediments overlaying two layers of early Upper Paleolithic artifacts, corresponding in raw material and form to those collected throughout the 20th century now in museum

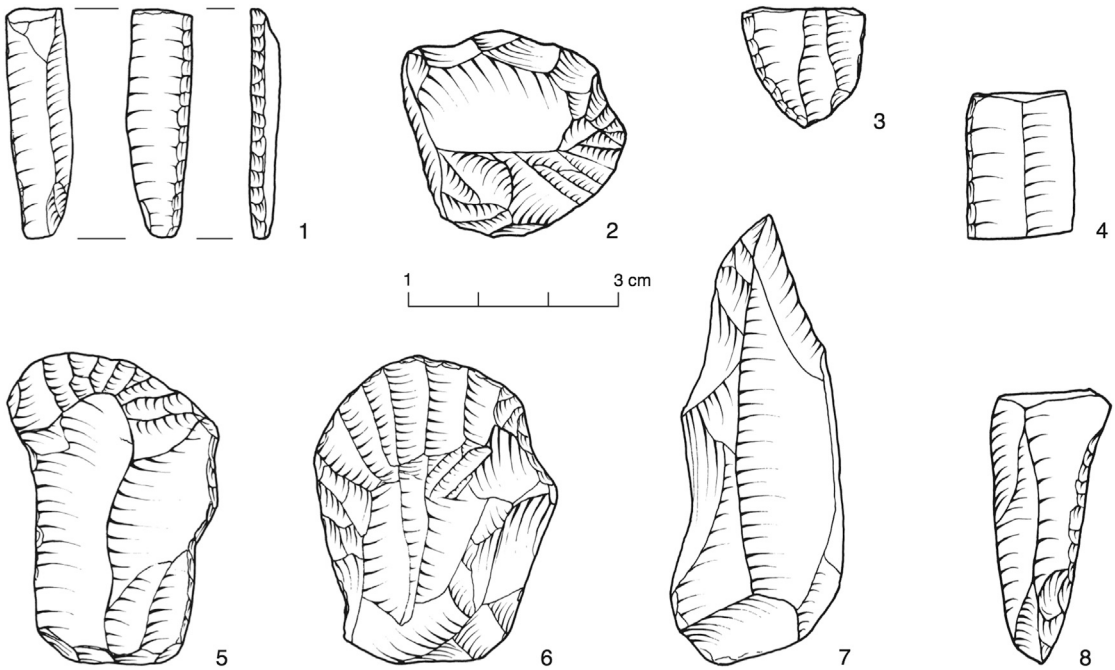

FIGURE 3 | Selected lithic artifacts from the Crvenka-At 2015 excavations (from Chu et al., 2016a).

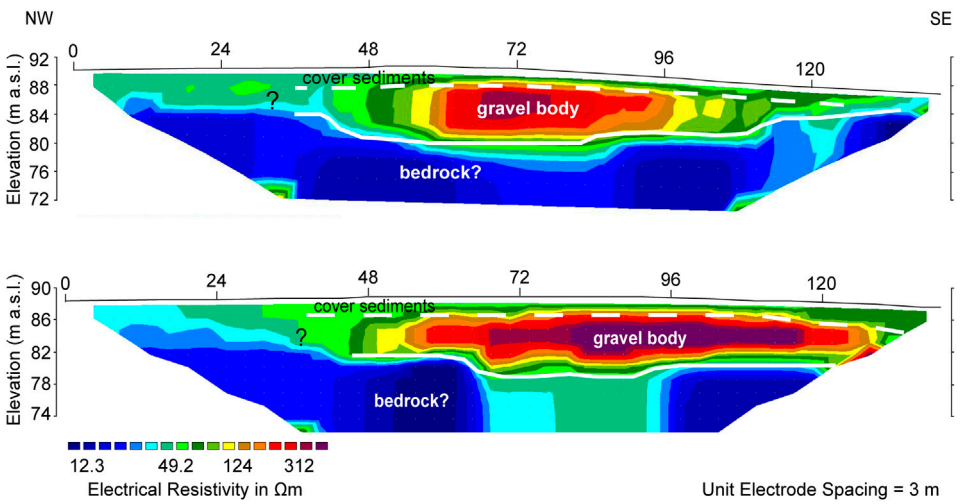

FIGURE 4 | Inversion models of ERT-transects CRV ERT 3 **(upper)** and CRV ERT 4 **(lower)**. The coarse-grained sediments that were found at the bottom of the excavation trenches are depicted by a unit of high resistivity values while overlying cover sediments show significantly lower resistivity values. The shape of these units indicates the presence of a fill terrace with overlying cover sediments. The base suggests incision into underlying strata at identical elevation AMSL. Stratigraphic information for the underlying units that are characterized by low resistivity values rising toward the northwest is not available. The location of the transects is depicted in **Figure 1C**.

collections. The artifacts were found in a relative depth of ~1.90 and ~2.05 m in trench 3 and ~3.90 m and ~4.10 m in trench 5 (~83 m AMSL). Excavations uncovered early Upper Paleolithic Aurignacian lithic artifacts (usually placed around 43–35 ka), including several bladelet cores (e.g., thick endscrapers, nosed endscrapers), blades and endscrapers (**Figure 3**). Most or all of the blades come from single-platform cores and the high blade-to-flake ratio of the lithic assemblage made primarily from so-called *Banat flint* (Ciornei et al., in press) that is technologically consistent with the Aurignacian artifacts from the open air sites of the Romanian Banat (Anghelinu et al., 2012; Sitlivy et al., 2012; Sitlivy et al., 2014; Chu et al., 2016b; Chu et al., 2019). Some of the

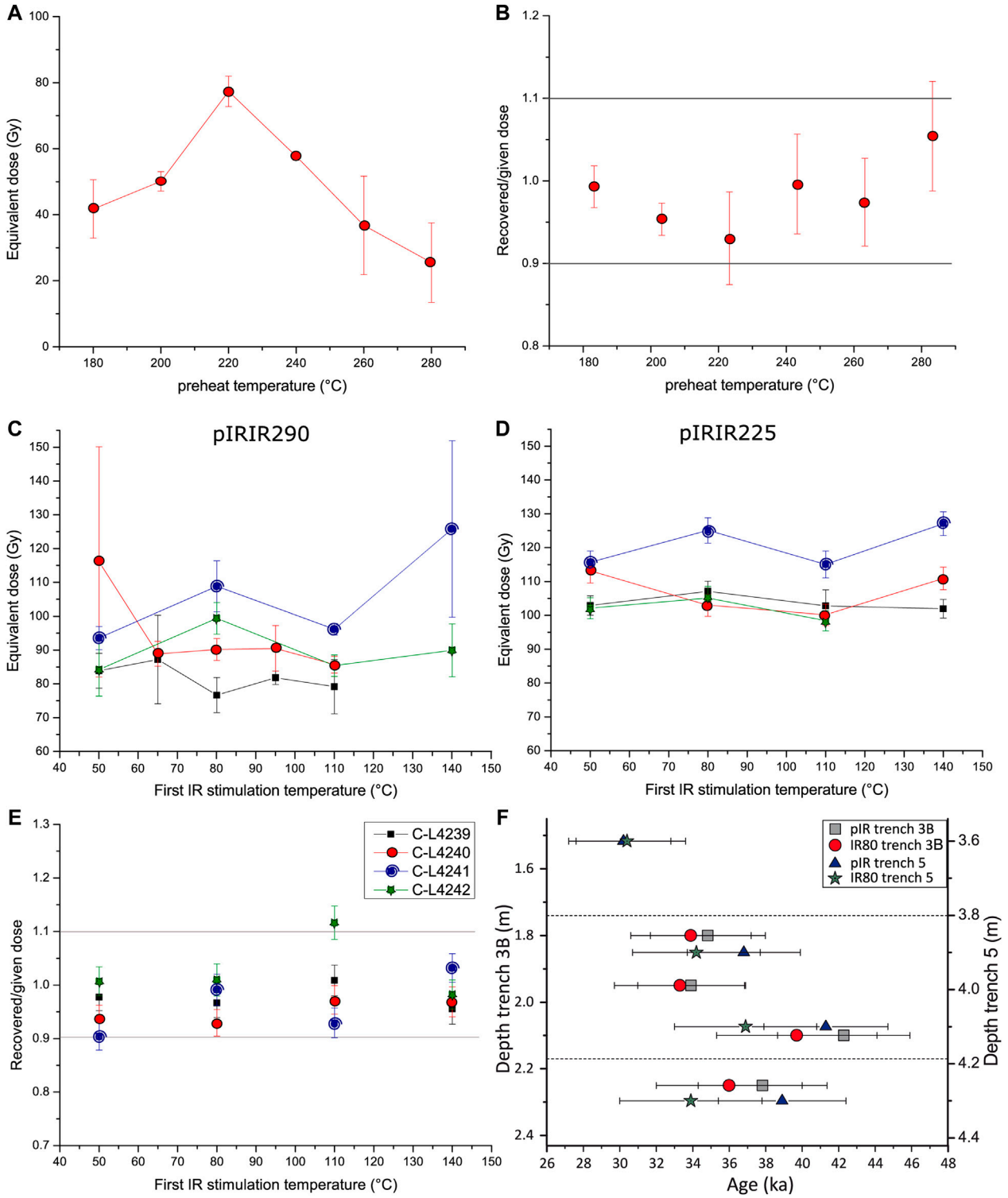

FIGURE 5 | Luminescence dating results from Crvenka-At. Preheat plateau test **(A)** and dose recovery test **(B)** of the quartz fraction of sample C-L4240; first IR stimulation temperature tests using the $pIRIR_{290}$ **(C)** and $pIRIR_{225}$ **(D)** protocols, dose recovery test **(E)** of the feldspar fractions of samples C-L4239–C-L4242, and age-depth plot showing the age data of the $pIRIR_{225}$ and the IR_{80} signals of all samples **(F)**.

lithics in the upper layer were recovered in sandy deposits and showed fine-grained fluvial abrasion (*sensu* Chu, 2016, p. 123), while others were found in fresher condition within finer-grained deposits. Bone preservation from these levels was infrequent and poor, however identified species include *Bos primigenius* and *Equus* sp. that were found in the find layers in trench 3. None of the remains retained suitable collagen for ^{14}C-dating.

Electrical Resistivity Tomography

ERT transects CRV ERT 3 and CRV ERT 4 (**Figure 4**) were conducted to obtain information on the near-surface stratigraphy of the site and its surroundings. In both transects, the lowest unit is characterized by low resistivity values sloping upward toward the northwest. On top, a unit of higher resistivity values is limited to the central and southeastern parts of the transects (from 48 m toward the end) showing a sharp lower boundary and a gradual transition to the overlying unit of lower resistivities. In the excavation area, the find layers occur within and on top of sandy gravels below a layer of finer sandy and silty sediments. The transition between these layers is marked by a gradual decrease of resistivities in both transects. The sharp lower boundary was not disclosed in the profile sections, thus no information on the strata characterized by low resistivities is available.

Luminescence Dating

The quartz fraction results were variable with some aliquots (2–8 mm) approaching saturation and exhibiting a small IR signal, although no feldspars were detected under the microscope. The measurements focused on the 100–150 µm grain size fraction. The preheat plateau test of sample C-L4240 did not show a plateau, but the dose recovery test behaved satisfactorily with recovered/given dose ratios between 0.95 ± 0.02 and 1.05 ± 0.07 (**Figures 5A,B**). The different characteristics of the single aliquots are demonstrated in **Supplementary Figure S3** that show shine down and dose response curves of three quartz aliquots from sample C-L4240. D_e measurements were performed with a preheat temperature of 240°C. However, the Abanico plot in **Supplementary Figure S4** demonstrates a large spread in the D_e data, as only 43.6% of the data points lie in a 2σ range. Due to this problematic behavior, the quartz fraction was not further measured.

For the potassium feldspar fraction of samples C-L4239–C-L4243, a first IR stimulation temperature test was conducted using the $pIRIR_{225}$ and the $pIRIR_{290}$ protocols (see **Figures 5C,D**). For the latter, no plateau region could be identified, but the $pIRIR_{225}$ showed less scatter with a first IR stimulation temperature plateau between all tested temperatures. Therefore, a dose recovery test was applied using solely the $pIRIR_{225}$ protocol. **Figure 5E** shows recovered/given dose ratios between 0.96 ± 0.03 and 1.12 ± 0.03. Fading measurements indicate low fading rates of g_{2days} = 0.08 ± 0.77% ($pIR_{50}IR_{225}$), g_{2days} = 0.01 ± 0.77% ($pIR_{80}IR_{225}$) and g_{2days} = 0.21 ± 0.78% ($pIR_{110}IR_{225}$; given as average and standard deviation; see **Supplementary Figure S5**). Due to the satisfactory behavior of the measurements using the $pIR_{80}IR_{225}$ protocol within the first IR stimulation temperature test, dose recovery test and fading experiment, the D_e measurements were also carried out with this protocol. **Supplementary Figures S6** and **S7** present shine down and growth curves for all measured samples from both trenches, which show bright luminescence signals. **Supplementary Figures S8** and **S9** depict the corresponding Abanico plots. There is variability in the data, but this is likely from the small aliquot sizes (2 mm) derived from coarse-grained sediments possibly transported by fluvial processes. A summary of the luminescence and age data is given in **Table 1** and the dose rate data of the sediment layers is given in **Table 2**. The saturation water content measurements indicate a value of ~24% for the sandy layer (unit C in **Figure 2**). To account for a range (50%) of possible moisture conditions, a water content of 12 ± 6% was used for all samples in the age calculations. A higher water content of 20 ± 8% was assumed for C-L4242 and C-L4246 from unit D, because the measured water contents were higher than within the other samples.

To further investigate the luminescence results, the IR_{80} signals contained in the $pIR_{80}IR_{225}$ measurements were analyzed (**Supplementary Figure S10**). Dose recovery ratios were satisfactory for all tested samples (average: 0.95 ± 0.04, **Supplementary Figure S11**). Equivalent doses were between 100 and 144 Gy. The fading rate for sample C-L4240 was with g_{2days} = 0.65 ± 0.70% slightly higher than for the pIRIR measurements (cf. **Supplementary Figure S12**). This value was used to correct the IR_{80} ages of all samples. The resulting fading corrected mean ages were all slightly younger than the corresponding pIRIR ages, but age estimates agreed within 1σ uncertainty (**Figure 5F**). A summary of the IR_{80} luminescence data is provided in **Supplementary Table S1**. **Figure 5F** shows an age-depth plot of the two profiles At I-3B and At I-5 and highlights the consistency between the obtained ages.

The age model places the sediment deposition of the dated samples between 38.9 ± 3.0 and 32.6 ± 2.5 ka (1σ; **Figure 6**, Tab. S2). The Aurignacian artifacts were found between samples C-L4240 and C-L4241 and C-L4244 and C-L4245, indicating the deposition of the find-bearing sediments according to the OSL data between 44.1 ± 3.4 and 33.9 ± 2.9 ka (1σ; cf. **Table 1**, **Supplementary Figure S13**). It should be noted that the timing can be pinpointed more precisely at At I-5, but more artifacts were found at At I-3B. Considering the age model, which incorporates the stratigraphic information (i.e., order of the samples), the sediments of the upper artifact level deposited at 35.3 ± 3.6 ka (2σ), while the lower level deposited between 35.3 ± 3.6 ka (2σ) and 37.8 ± 4.2 ka (2σ). Averaging all the modeled ages within the archeological context, gives an overall modeled average timing of 36.4 ± 2.8 ka (2σ).

Grain Size Analysis

Grain sizes were clustered into four units related to their stratigraphy and textural characteristics (see **Figure 7**). The most completely sampled trench 3A (**Figure 7A**) shows a well-sorted pattern in all units. The upper unit (0.00–1.20 m) depicts a bimodal grain size distribution (GSD) with a minor peak in coarse silt and a distinct peak in medium sand. A shoulder in medium and coarse clay can be also observed. Unit B (1.20–1.75 m) shows a similar pattern, but here the sand

TABLE 1 | Summary of the luminescence data of the potassium feldspar samples from At trench 5 and trench 3B. The used grain size (GS), depth considering erosion of ~1.6m, number of accepted (n) and measured (N) aliquots measured (W_m) and used (W_{used}) water contents, cosmic (D_{cos}) and total dose rates (D_{total}), residual doses, equivalent doses (D_e) and ages are shown.

Code C-L	GS (μm)	Depth (m)	*n/N*	W_m (%)	W_{used} (%)	D_{cos} (mGy/ka)	D_{total} (Gy/ka)	Residual (Gy)	D_e (Gy)	Age (ka)
4239	150–200	3.6	28/34	8	12 ± 6	143	3.33 ± 0.34	1.4 ± 0.1	100.62 ± 5.25	30.2 ± 2.6
4240	150–200	3.9	43/46	3	12 ± 6	139	2.81 ± 0.28	1.3 ± 0.2	103.60 ± 5.67	36.8 ± 3.1
4241	100–250	4.1	28/34	1	12 ± 6	136	2.85 ± 0.28	1.3 ± 0.1	118.00 ± 6.11	41.3 ± 3.4
4242	150–200	4.3	30/31	20	20 ± 8	133	2.57 ± 0.27	1.4 ± 0.1	100.04 ± 5.12	38.9 ± 3.5
4243	150–200	3.1	36/37	8.3	12 ± 6	150	3.25 ± 0.35	1.3 ± 0.2	113.1 ± 6.83	34.8 ± 3.2
4244	150–200	3.3	39/40	3.8	12 ± 6	148	3.25 ± 0.33	1.4 ± 0.1	110.05 ± 5.96	33.9 ± 2.9
4245	150–200	3.5	51/55	5.7	12 ± 6	144	3.85 ± 0.41	1.4 ± 0.1	158.84 ± 9.24	41.3 ± 3.6
4246	150–200	3.7	32/34	13.4	20 ± 8	142	3.13 ± 0.34	1.3 ± 0.1	118.23 ± 6.45	37.8 ± 3.5

TABLE 2 | Summary of the dose rate data shown for the individual stratigraphic layers of At trench 5 and trench 3B.

Layer	U (Bq/kg)	Th (Bq/kg)	K (Bq/kg)
At1-5A	20.71 ± 1.01	25.34 ± 1.31	636.29 ± 9.46
At1-5B	4.93 ± 0.43	6.96 ± 0.51	647.13 ± 9.49
At1-5C	5.51 ± 0.42	6.66 ± 0.48	686.17 ± 9.98
At1-5D	4.58 ± 0.35	5.85 ± 0.46	645.46 ± 9.52
At1-3B A	20.91 ± 1.07	23.97 ± 1.30	613.94 ± 9.15
At1-3B	12.43 ± 0.72	15.67 ± 0.94	713.57 ± 10.38
At1-3B C	6.62 ± 0.54	10.12 ± 0.71	1,024.52 ± 14.37
At1-3B D	12.68 ± 0.73	17.89 ± 1.02	712.63 ± 10.49

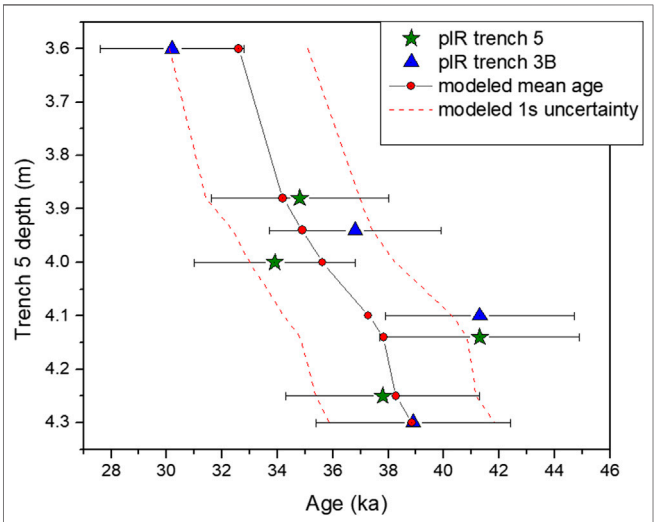

FIGURE 6 | Age-depth plot showing the pIR ages (green stars, blue triangles), the modeled mean ages (red circles), and their upper and lower 1σ of credibility (dashed red lines).

fraction is divided into two peaks at ca. 245 and 567 μm. The clay content of Unit C (1.75–2.08 m) is lower than in units A and B and three local maxima are found at 35, 200, and 517 μm. Unit D (2.08–2.3 m) is composed of fine and medium sand with a bimodal distribution that peaks around 170–180 and 567 μm as well as negligible amounts of clay and silt.

Despite its proximity to profile 3A (ca. 1.5 m), profile 3B shows a different pattern (**Figure 6B**). The GSD is poorly-sorted and the sediments are generally coarser than in profile 3A. While the GSD of units A and B (0.90–1.56 m) show minor contributions of clay and silt, these are absent in units C (1.50–1.78 m) and D (1.78–2.14 m). All units are primarily comprised of coarse sands, but also show high values of fine and medium sand.

Grain sizes of profile 5 show a well-sorted distribution (**Figure 7C**). Unit A (3.60–3.87 m) is characterized by a trimodal distribution with peaks in coarse silt (ca. 35 μm), fine (ca. 200 μm) and medium sand (517–623 μm). Unit B cannot be clearly identified, but the upper part of unit C (3.87–4.03 m) shows small amounts of silt and medium sand (623 μm) and may be contemporary to unit B. The rest of unit C shows a GSD that generally peaks in medium and coarse sand (684–993 μm). The GSD of the lowermost sample (only representative of unit D in this profile) peaks in fine sand (140 μm) with a shoulder in medium sand.

Sediment profiles 3A and 3B were correlated based on stratigraphy and grain size data. The mode of the grain size shows good agreement between the profiles (see Fig. S14). Further details on the in-depth variations are depicted in **Figures 8**, **9**.

Spectrophotometric Analysis

The color data of trenches 3A and B follow the same pattern with high L*, a* and b* values in unit D and decreased values in unit C. a* and b* are elevated again in unit B and fluctuate slightly in unit A. L* is slightly lower in unit B than A and decreases at the top of profile 3A. Mean values are 59/62 (L*), 2/1 (a*) and 17/15 (b*) for trenches 3A and 3B, respectively (**Figure 8**).

The color data of trench 5 shows less fluctuations than in trench 3. L* has a decreasing trend in the lower 10 cm, which is followed by a gradual increase. At ~490 cm, values drop sharply to be followed by a gradual increase again. The mean L* value is 63. a* and b* show a similar pattern with local maxima at 396 and 418 cm. The upper 36 cm have an increasing trend in b*. Mean a* and b* values are 2 and 18. See **Figure 9** for full details.

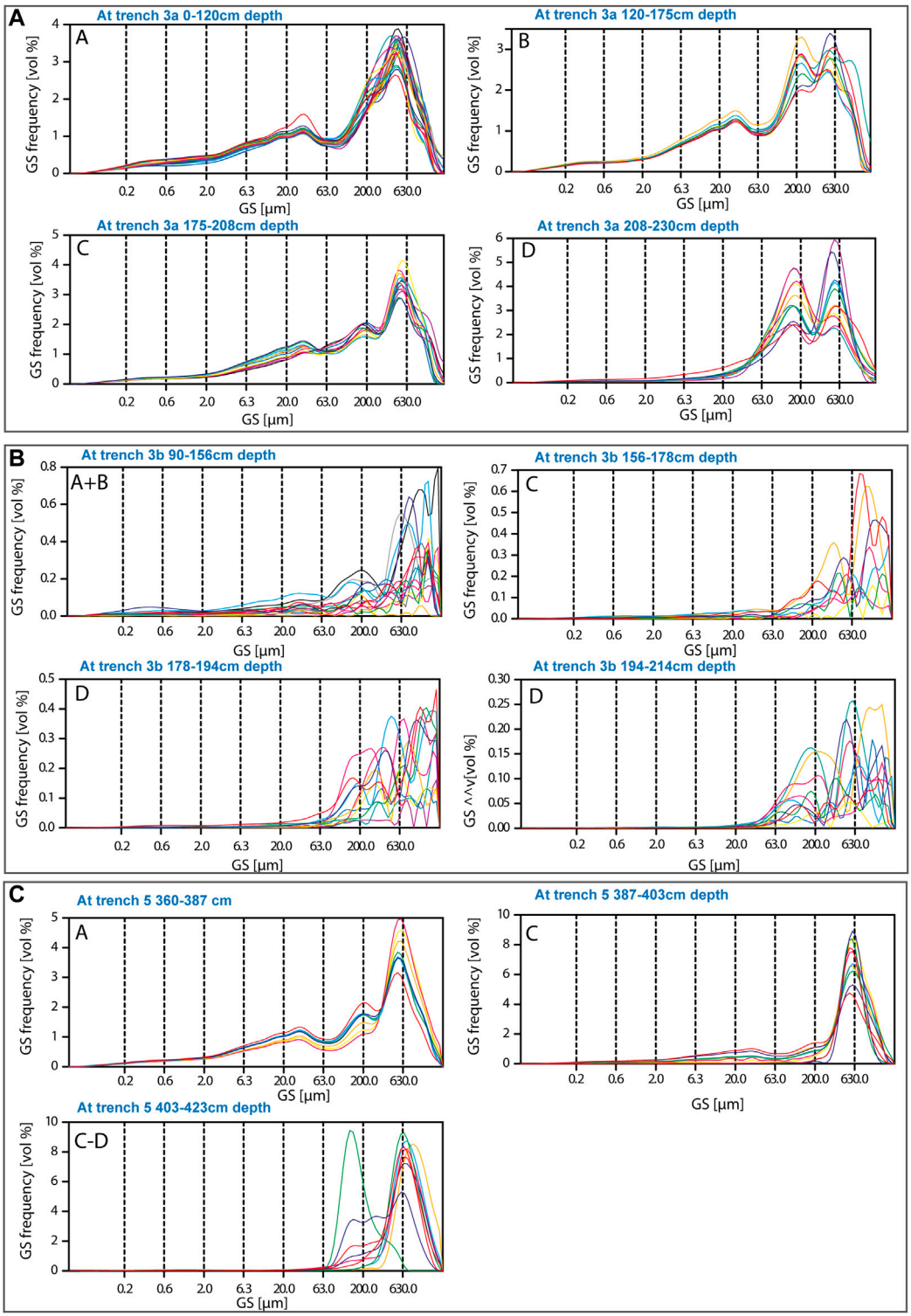

FIGURE 7 | Grain size distribution of At trench 3A **(A)**, trench 3B **(B)**, and trench 5 **(C)**. Position according to stratigraphy is indicated by **A–D**; see **Figure 2**. In trench 5 only one sample represents the fine white sands of unit D because sampling did not continue further down. Random colors are used to differentiate between the single samples.

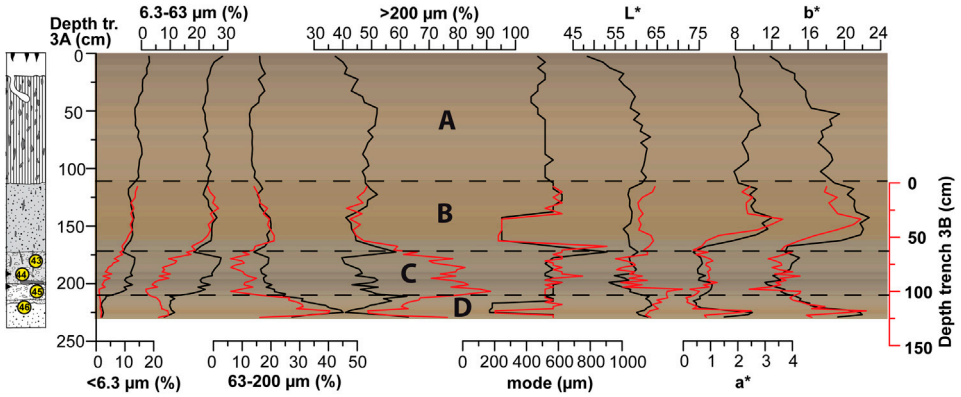

FIGURE 8 | Proxy data of At trench 3A (black line) and 3B (red line) show the grain size distribution in classes <6.3, 6.3–63, 63–200, and >200 µm, and the mode. Further, spectrophotometric color data (L, a*, b*) is shown. Measured colors are plotted in the background using the 'drawProfile.R' R script (Sprafke, 2016; Zeeden et al., 2017). A simplified sketch of the stratigraphy is shown on the left and the stratigraphic units are indicated by A–D (see legend in **Figure 2**).

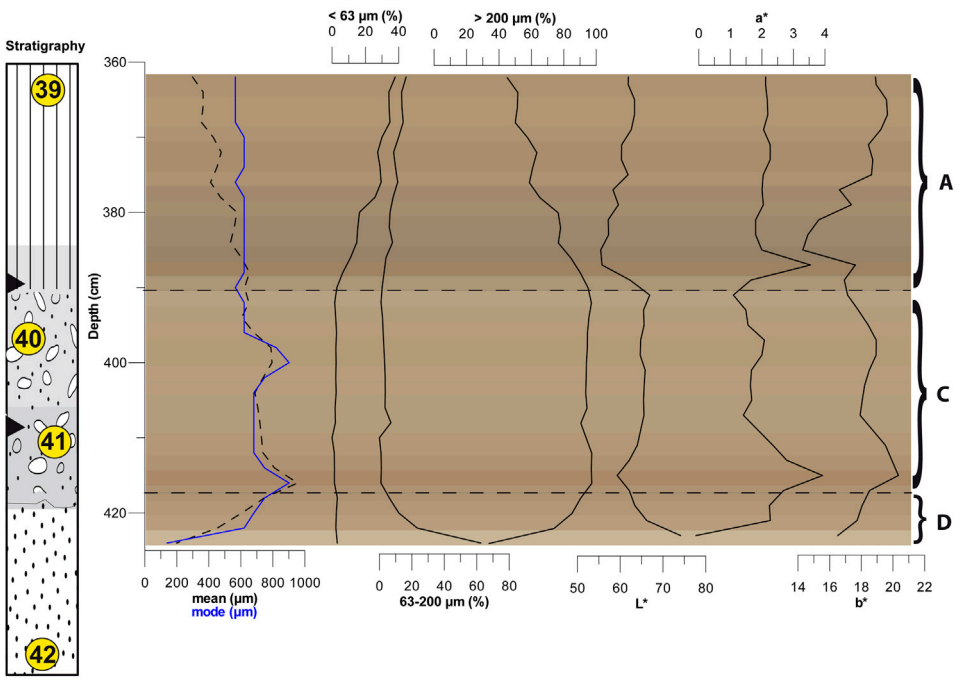

FIGURE 9 | Proxy data of At trench 5 showing the mean and mode, grain size distribution in classes <63, 63–200, and >200 µm and the spectrophotometric color data (L, a*, b*). Measured colors are plotted in the background using the 'drawProfile.R' R script (Sprafke, 2016; Zeeden et al., 2017). A simplified sketch of the stratigraphy is shown on the left and the stratigraphic units are indicated by A–D (see legend in **Figure 2**).

DISCUSSION

Geochronology

After thorough investigation of the quartz and potassium feldspar luminescence characteristics, it was shown that the $pIR_{80}IR_{225}$ protocol using potassium feldspars is most suitable for D_e measurements. The problematic behavior of the quartz fraction (i.e. approaching saturation, IR signal, wide scatter, no preheat plateau) might be due to metamorphic source rocks, which are fairly abundant in the Vršac Mountains. Additionally, the OSL samples contained a high amount of muscovite, which were difficult to remove during sample preparation. While quartz crystals sourced from metamorphic rocks reportedly are affected by problematic luminescence behavior (cf. Nelson et al., 2015), the occurrence of IR signals might also point to feldspar inclusions within the quartz crystals, but this was not investigated further. Popov et al. (2012) who investigated late glacial fluvial terrace deposits of the Tisza River in northern

Serbia encountered complex luminescence characteristics in their quartz samples. Most of their aliquots exhibit an IR signal, which they tried to remove using a double-SAR protocol (Banerjee et al., 2001), prior to the D_e measurements. However, even then large variability between aliquots and shine down curve shapes as well as poor recycling ratios were observed. In a later study, this complex behavior was not encountered, but overestimated dose recovery ratios led the authors to caution the quartz OSL results (Vandenberghe et al., 2018).

The potassium feldspar samples, however, showed excellent luminescence characteristics. Our samples exhibit no laboratory fading, even though fading rates have been reported in literature (Vasiliniuc et al., 2012). Residual doses are <1.5 Gy. Also the IR_{80} signal shows little fading and the fading corrected ages agree within 1σ uncertainty with the $pIRIR_{225}$ ages. The difference between both sets of ages is slightly higher in samples C-L4240–C-L4242 and C-L4245, which may be due to a minor degree of incomplete bleaching (cf. Murray et al., 2012; Klasen et al., 2018) or the fading correction (cf. Thomsen et al., 2008; Guérin et al., 2015). Further uncertainty is likely introduced by the estimation of the moisture content. Therefore, the saturation water content was determined to achieve a better estimate of the average moisture conditions since deposition. Nevertheless, some uncertainty remains because this was only done for one sample. This uncertainty might also explain why in both profiles, the lowermost samples from layer D have slightly younger mean ages than the samples above. Here, also the measured water content was higher than within the other samples. Of course, one might also argue that the age estimates of samples C-L4241 and C-L4245 are overestimated, but this seems unlikely considering that their ages are identical. Nevertheless, when the Bayesian age model is applied, it shifts these ages to their lower uncertainty limit (cf. **Figure 6**).

Although the luminescence tests (first IR stimulation temperature tests, dose recovery tests and fading experiments) were only carried out on the samples of At I-5, the geochronologies of both profiles agree. This further supports the robustness of the luminescence ages. Nevertheless, the Abanico plots (**Supplementary Figures S8** and **S9**) show more scatter in the D_e distributions of the samples from At I-3B, which is likely connected to post-depositional mixing due to rootlet penetration (as observed in the field) and/or may be linked to the unsorted grain size distributions (**Figure 7**). However, most D_e distributions resemble a normal distribution and only samples C-L4240 and C-L4245 show a skewed distribution toward higher D_e values. Nevertheless, this does not significantly affect the average D_e and only a few outliers are present (cf. **Supplementary Figures S8** and **S9**). Our investigation shows that potassium feldspars at Crvenka-At can be successfully dated using the $pIRIR_{225}$ protocol. This shows potential for other studies on coarse-grained feldspars in the Carpathian Basin, as was already suggested for the deposits of the paleo Tisza River (cf. Popov et al., 2012; Vandenberghe et al., 2018). Nevertheless, it should be noted that the dated grain size fraction does not reflect the dominant sedimentological grain size (cf. **Figure 7**).

Age modeling of the luminescence age data reduced the overall uncertainty and evened out some age estimates (**Figure 6**). For example, the ages of samples C-L4239 and C-L4244 are modeled to be slightly older, while the ages of samples C-L4241 and C-L4245 are modeled to be younger. It also allowed for more precise age estimates for the artifact layers.

Environmental and Geomorphological Evolution

The results from the ERT-measurements characterized the sedimentary composition of the shallow subsurface at the study site, allowing the identification of the broader stratigraphic context. The find-bearing layers occur in sand-dominated, in parts gravelly, deposits that are depicted by relatively high resistivity values (up to 300 Ωm in CRV ERT 3; **Figure 4**). The sharply developed lower boundary of this unit probably indicates an erosional phase cutting into the underlying strata followed by an accumulation of sand and gravel (as evident in the trenches). Shape and distribution are indicative of a fill terrace. Remarkably, the deepest incision does not occur downslope but in the center of the ERT-transects. Thus, it is possible that erosion and accumulation of the coarser grained material was related to fluvial (channeled) runoff evidenced by high resistivity values followed by the accumulation of overbank deposits. There are no other ERT studies conducted in this region, but the observed values compare well to the cover sediments on top of fluvial terraces in the Rhine area (Gerlach, 2019; Fischer et al., 2021).

Based on the sediment characteristics (**Figures 7–9**), the drainage patterns and the overall geomorphology, one can presume that the sediments were related to fluvial deposition close to a river mouth draining into a paleolake in the Alibunar Depression. This is similar to the morass mapped by Müller (1769) and will be investigated in a forthcoming publication (Zeeden et al., 2021). Additionally, a differentially compaction may have influenced the bedding inclination toward finer grained sedimentary units as they undergo higher compaction than sandy and gravelly units (e.g., Bjørlykke, 2015).

Similar to the ERT-measurements, the grain size data shows coarser sandy and gravelly deposits in units C and D and finer deposits in units A and B. The GSD of trench 3A, with its peaks in coarse silt and medium sand, can be interpreted as reworked sand (cf. Chu et al., 2019). The GSD of trench 3B points to fluvial sand deposits, shown by high amounts of poorly-sorted fine to coarse sands. Variations in grain sizes in unit C and the clast-supported appearance point to higher transport velocities during deposition in comparison to unit D, where the mode of the grain size decreases in both trenches. The grain size differences within trench 3 can be interpreted as contrasting depositional environments typically occurring alongside fluvial channels, at lakeshores or in alluvial fan or delta settings (cf. Xiao et al., 2012; Brooke et al., 2018; Vandenberghe et al., 2018). The absence of finer material such as silt in units C–D of trench 5 highlights that the fluvial sedimentary system was complex, even at a local scale. The relatively well sorted GSD, especially GSD, especially in unit A of trench 5, might point to an eolian origin of these sediments, while the GSD of this unit in trench 3 is more turbulent, possibly confirming the interpretation of overbank deposits.

The consistency of bleaching/graying as seen in the field and imprinted in decreased L* and b* values (unit C; **Figures 7**, **8**) is interpreted as post-depositional hydromorphic alteration of the sediments. It implies phases of water saturation at least in trench 3 (compare color data in **Figures 8**, **9**). This might be related to high groundwater tables or slack water conditions in the vicinity of a water body and close to a groundwater table little below the land surface. Moreover, elevated a* and b* values in unit B indicate preservation or subsequent formation of iron (hydr-) oxides such as hematite (tentatively indicated by a*) and goethite (tentatively indicated by b*) due to *in situ* weathering (Barron and Torrent, 1986). The fine material in units B and A suggests a low energy deposition that might have occurred in a less fluvial and possibly (episodic) overbank or lacustrine environment. Additional eolian sediment input might have been possible. These sediments were subsequently heavily bioturbated, which is especially evident in trench 3.

Additionally, the observed bones of *Bos primigenius* and *Equus sp.* found in the artifact levels of trench 3 may suggest a general limnic/fluvial woodland environment: *Bos primigenius* preferred floodplain habitats in river valleys, river deltas and bogs (Tikhonov, 2008) and the occurrence of *Equus sp.* suggests a grass-dominated habitat in proximity. While this needs to be considered with caution, as only two identifiable faunal fragments were found, it matches well with our sedimentological interpretation of a river stream (units D, C) changing toward a floodplain or lakeshore environment (units B, A). From a sequence stratigraphic point this change in time will apply to space as well, inferring overbank or lakeshore sediments in the vicinity.

Changes in fluvial systems in this complex setting (see *Geological and Geomorphological Setting section*) do not readily correlate to climatic changes (cf. Starkel et al., 2015) and we can expect that large rivers, oxbow lakes or lakes were likely always present in tectonic depressions such as Alibunar Nevertheless, the timing of fluvial sediment deposition (~42–31 ka; units D-C) coincides with the formation of Middle Pleniglacial (MIS 3) paleosols and pedocomplexes of the southern Carpathian Basin (e.g., Fuchs et al., 2008; Antoine et al., 2009; Schmidt et al., 2010; Zeeden et al., 2016; Avram et al., 2020). This suggests a phase of warmer and moister climatic conditions with higher fluvial discharge velocities, although the southern parts of the Carpathian Basin were generally arid (e.g., Obreht et al., 2019). For unit A and B, only one date of 30.2 ± 2.6 ka is available, thus, we cannot infer much. It is possible that the upper non-investigated parts of the trenches were formed during MIS 2, when loess sedimentation is reported in the region (e.g., Marković et al., 2014; Obreht et al., 2015; Marković et al., 2018; Perić et al., 2019; Perić et al., 2020). This might be connected to enhanced eolian sand and silt input at Crvenka-At as suggested by the well-sorted GSDs (trench 5), but needs further investigation.

Archeological and Paleoanthropological Implications

The results indicate that Aurignacian artifacts at Crvenka-At were found in sediments that accumulated 36.4 ± 2.8 ka (2σ modeled ages). With this, the assemblages are firmly ascribed to MIS 3 and correspond with the nearby early modern human remains from the Peştera cu oase (ca. 42–37 ka cal BP[1]; Trinkaus et al., 2003a; Trinkaus et al., 2012), the Peştera Muierii (ca. 35 ka cal BP; Soficaru et al., 2006) and the Peştera Cioclovina (ca. 35.5 ka cal BP; Soficaru et al., 2007). If the full range of the OSL ages is considered, these additionally overlap with other dated Aurignacian sites in the Banat at Românești (40.6 ± 1.5 ka; Schmidt et al., 2013), the small (<15 artifacts) assemblages from the Baranica Cave (layer 4b; 40.76 ± 0.73 ka cal BP, Mihailović et al., 2011), Tabula Traiana Cave (Layer 207; 41.3 ka cal BP to 34.5 ka cal BP; Borić et al., 2012; Mandić and Borić, 2015) and the poorly-contextualized Peştera Hoţilor (30.90 ± 0.37 ka cal BP; Anghelinu and Niţă, 2014; Păunescu, 2001, p. 142).

Crvenka-At's main interest is its lowland setting; an outlier in the Carpathian Basin's Aurignacian record. While lowland Aurignacian sites are occasionally encountered elsewhere in Europe (e.g., Masières Canal; Miller, 2014), it has previously been suggested that the occurrence of Aurignacian sites in short stratigraphic sequences in the Carpathian Basins foothills, between 43 and 30 ka BP are a genuine reflection of modern human behavioral preference for this specific biome (Hauck et al., 2018). Our results provide a first direct indication that modern humans made use of riparian landscapes possibly to avoid mountainous regions as a result of late Neanderthal territoriality until c. 39 ka cal BP in the Central Balkans (Alex, 2016, 112; Marín-Arroyo and Mihailović, 2017; Alex et al., 2019; Mihailović, 2020). In the Banat however, the situation may have been more nuanced given the recent Neanderthal/modern human hybridization at the Peştera cu oase in the nearby Anina Mountains indicating territorial and temporal overlap (Fu et al., 2015).

Our results also suggest that fluviolacustrine environments were exploited by early modern humans potentially even representing a favorable location in the landscape where vital aquatic food sources rich in micronutrients could be harvested (Brown et al., 2013). Two technologically analogous layers at At along the wider Crvenka-At complex suggest multiple site visits or at least a more sustained occupation of the area. This is in agreement with isotopic findings from the region's early Upper Paleolithic human record that have high δ^{15}N values, suggesting higher consumption of freshwater foods compared to previous indigenous populations (Richards and Trinkaus, 2009; Trinkaus et al., 2009).

Excavation results thus document the site formation processes of Crvenka-At and interpret the site as a palimpsest of a series of hominin visits of short duration captured within fine-grained, water-lain sediments. This highlights the potential for finding large, well-preserved Late Pleistocene archeological sites within the Carpathian Basin lowlands that may provide important archaeological context (Fitzsimmons et al., 2020) and recommends further (geo)archeological work in these environs to fill the current

research gap. All radiocarbon ages were calibrated using Calpal2007-Hulu (Weninger et al., 2008)

CONCLUSION

We confirm and date the Aurignacian site of Crvenka-At in the Banat region of the southeastern Carpathian Basin using luminescence dating of potassium feldspars. The Aurignacian artifacts were found in sediments with a modeled age of 36.4 ± 2.8 ka (2σ). This age range agrees with other dated Aurignacian findings in the Banat region and further confirms the early chronological position of the Aurignacian in the Carpathian Basin. Moreover, it is suggested that the site served for repeated/sustained hominin visits as evidenced by numerous multi-layered find spots within the sand ridge. The combination of ERT and sedimentological analyses confirm a position of the site within a complex fluviolacustrine environment. Shape and distribution of the ERT-transects suggest an interpretation as sandy-gravelly fill terrace and also the diverse grain-size distribution of the investigated trenches support a formation within fluvial channels, at lakeshores or in alluvial fan or delta settings. Subsequent weathering and phases of water saturation further altered the deposited sediments. Further association to a potential paleolake needs to be investigated in future studies. Our study demonstrates that not only the upland regions, but also lowland areas were attractive to early modern human hunter-gatherers and demonstrates the need for more comprehensive geoarcheological investigations including the analyses of different sedimentary archives.

DATA AVAILABILITY STATEMENT

Granulometric and colorimetric data analyzed for this study are reposited in the CRC806 Database (https://doi.org/10.5880/SFB806.62). For luminescence data, please consult the **Supplementary Material**. Further inquiries can be directed to the corresponding author.

AUTHOR CONTRIBUTIONS

JN, WC, CZ, PF, UH, and FL contributed conception and design of the study. JN, CZ, UH, IO, PF, and LO conducted sediment sampling and ERT measurements. WC and DM undertook archeological excavation and interpretation. PF, LO and AV analyzed and interpreted the ERT data. JN undertook OSL sample preparation, measurements and analysis with support and discussion by NK. JN analyzed and interpreted the grain size and color data with support and discussion by SP and IO. JN wrote the first draft of the manuscript. PF and WC wrote sections of the manuscript. All authors were involved with the regional discussion and interpretation. All authors contributed to manuscript revision, read and approved the submitted version.

FUNDING

The investigations were carried out in the frame of the CRC 806 "Our Way to Europe", subproject B1 "The Eastern Trajectory": "Last Glacial Palaeogeography and Archaeology of the Eastern Mediterranean and of the Balkan Peninsula", funded by the Deutsche Forschungsgemeinschaft (DFG, German Research Foundation)–Projektnummer 57444011-SFB 806. The work of DM was supported by Ministry of Culture and Information and the Ministry of Education, Science and Technological Development of the Republic of Serbia (project no. 177023).

ACKNOWLEDGMENTS

We thank Ivana Pantović, Nadine Nolde, Dragan Jovanović for their gracious help in the field and laboratory; Anja Zander for the dosimetry measurements and support in the Cologne Luminescence Laboratory, Marianne Dohms and the PGG team for the measurements of the grain size and color data and Philipp Schulte for support in the analysis of the grain size data. We thank Jens Weise for his work on **Figure 1**; **Supplementary Figure S1**, Thomas Albert on **Figure 1C** and Anja Rüschmann and Sofija Dragosavac for drawing **Figure 3**.

SUPPLEMENTARY MATERIAL

The Supplementary Material for this article can be found online at: https://www.frontiersin.org/articles/10.3389/feart.2021.599986/full#supplementary-material.

REFERENCES

Alex, B. (2016). Establishing contexts of encounters: radiocarbon dating of archaeological assemblages with implications for Neanderthal-modern human interactions. Doctoral dissertation: Cambridge: Harvard University.

Alex, B., Mihailović, D., Milošević, S., and Boaretto, E. (2019). Radiocarbon chronology of middle and upper paleolithic sites in Serbia, central Balkans. *J. Archaeol. Sci. Rep.* 25, 266–279. doi:10.1016/j.jasrep.2019.04.010

Anghelinu, M., Niță, L., Sitlivy, V., Uthmeier, T., and Băltean, I. (2012). Looking around Peştera Cu Oase: the beginnings of upper paleolithic in Romania. *Quat. Int.* 274, 136–157. doi:10.1016/j.quaint.2012.01.012

Anghelinu, M., and Niță, L. (2014). What's in a name: the Aurignacian in Romania. *Quat. Int.* 351, 172–192. doi:10.1016/j.quaint.2012.03.013

Antoine, P., Rousseau, D.-D., Fuchs, M., Hatté, C., Gauthier, C., Marković, S. B., et al. (2009). High-resolution record of the last climatic cycle in the southern Carpathian Basin (Surduk, Vojvodina, Serbia). *Quat. Int.* 198, 19–36. doi:10.1016/j.quaint.2008.12.008

Avram, A., Constantin, D., Veres, D., Kelemen, S., Obreht, I., Hambach, U., et al. (2020). Testing polymineral post-IR IRSL and quartz SAR-OSL protocols on Middle to Late Pleistocene loess at Botanica, Serbia. *Boreas* 49, 12442. doi:10.1111/bor.12442

Banerjee, D., Murray, A. S., Bøtter-Jensen, L., and Lang, A. (2001). Equivalent dose estimation using a single aliquot of polymineral fine grains. *Radiat. Meas.* 33, 73–94. doi:10.1016/S1350-4487(00)00101-3

Barron, V., and Torrent, J. (1986). Use of the Kubelka—munk theory to study the influence of iron oxides on soil colour. *J. Soil Sci.* 37, 499–510. doi:10.1111/j.1365-2389.1986.tb00382.x

Bartha, A., Balázs, A., and Szalay, Á. (2018). On the tectono-stratigraphic evolution and hydrocarbon systems of extensional back-arc basins: inferences from 2D basin modelling from the Pannonian Basin. *Acta Geod. Geophys.* 53, 369–394. doi:10.1007/s40328-018-0225-0

Bjørlykke, K. (2015). "Compaction of sedimentary rocks: shales, sandstones and carbonates," in *Petroleum geoscience* (Berlin, Heidelberg: Springer), 351–360.

Borić, D., Dimitrijević, V., White, D., Lane, C., French, C., and Cristiani, E. (2012). Early modern human settling of the danube corridor: the middle to upper palaeolithic site of tabula traiana cave in the danube gorges (Serbia). *Antiq. Proj. Gallery* 86 (334).

Bösken, J. J. (2020). Luminescence dating of eolian and fluvial archives in the middle and lower danube catchment and the palaeoenvironmental implications. *E&G Quat. Sci. J.* 69, 89–92. doi:10.5194/egqsj-69-89-2020

Brooke, S. A. S., Whittaker, A. C., Armitage, J. J., D'Arcy, M., and Watkins, S. E. (2018). Quantifying sediment transport dynamics on alluvial fans from spatial and temporal changes in grain size, Death Valley, California. *J. Geophys. Res. Earth Surf.* 123, 2039–2067. doi:10.1029/2018JF004622

Brown, A. G., Basell, L. S., Robinson, S., and Burdge, G. C. (2013). Site distribution at the edge of the Palaeolithic world: a nutritional niche approach. *PLoS One* 8, e81476. doi:10.1371/journal.pone.0081476

Buylaert, J.-P., Jain, M., Murray, A. S., Thomsen, K. J., Thiel, C., and Sohbati, R. (2012). A robust feldspar luminescence dating method for Middle and Late Pleistocene sediments: feldspar luminescence dating of Middle and Late Pleistocene sediments. *Boreas* 41, 435–451. doi:10.1111/j.1502-3885.2012.00248.x

Buylaert, J. P., Murray, A. S., Thomsen, K. J., and Jain, M. (2009). Testing the potential of an elevated temperature IRSL signal from K-feldspar. *Radiat. Meas.* 44, 560–565. doi:10.1016/j.radmeas.2009.02.007

Chapman, J. (2000). *Fragmentation in Archaeology: people, places, and broken objects in the prehistory of south eastern Europe*. London; New York: Routledge.

Chu, W. (2016). *Fluvial processes in the Pleistocene of northern Europe*. Oxford: British Archaeological Reports.

Chu, W., Hauck, T., and Mihailović, D. (2014). "Crvenka-At– preliminary results from a lowland Aurignacian site in the Middle danube catchment," in *Palaeolithic and mesolithic research in the central Balkans*. Editors D. Mihailovic (Belgrade, Serbia: Serbian Archaeological Society), 69–75.

Chu, W., Mihailović, D., Pantović, I., Zeeden, C., Hauck, T., and Lehmkuhl, F. (2016a). Archaeological excavations at the site of at (Vršac, Serbia). *Antiq. Proj. Gallery* 90 (352).

Chu, W., Pötter, S., Doboș, A., Albert, T., Klasen, N., Ciornei, A., et al. (2019). Geoarchaeology and geochronology of the Upper Palaeolithic site of Temereşti Dealu Vinii, Banat, Romania: site formation processes and human activity of an open-air locality. *Quartär* 66, 111–134. doi:10.7485/QU66_5

Chu, W. (2018). The danube corridor hypothesis and the Carpathian Basin: geological, environmental and archaeological approaches to characterizing aurignacian dynamics. *J. World Prehist.* 31, 117–178. doi:10.1007/s10963-018-9115-1

Chu, W., Zeeden, C., and Petrescu, S. (2016b). The early upper paleolithic of the Banat and recent research at the paleolithic site of Tincova. *Banatica* 26, 51–72.

Ciornei, A., Chu, W., Maris, I., and Dobos, A. *(in press) Lithic raw material patterns at the Upper Palaeolithic site of Românești-Dumbrăvița* (Southwestern Romania). Dacia.

Conard, N. J., and Bolus, M. (2008). Radiocarbon dating the late middle paleolithic and the aurignacian of the swabian jura. *J. Hum. Evol.* 55, 886–897. doi:10.1016/j.jhevol.2008.08.006

Davies, W., White, D., Lewis, M., and Stringer, C. (2015). Evaluating the transitional mosaic: frameworks of change from neanderthals to *Homo sapiens* in eastern Europe. *Quat. Sci. Rev.* 118, 211–242. doi:10.1016/j.quascirev.2014.12.003

Doboș, A., and Chu, W. (2019). Between the woods and the water: the early Upper Palaeolithic from the Romanian karst. *Analele Banatului* 26, 17–34. Essays in honor of Alexandru Szentmiklosi.

Eckmeier, E., Mavris, C., Krebs, R., Pichler, B., and Egli, M. (2013). Black carbon contributes to organic matter in young soils in the Morteratsch proglacial area (Switzerland). *Biogeosciences* 10, 1265–1274. doi:10.5194/bg-10-1265-2013

Fischer, P., Jöris, O., Fitzsimmons, K. E., Vinnepand, M., Prud'homme, C., Schulte, P., et al. (2021). Millennial-scale terrestrial ecosystem responses to upper Pleistocene climatic changes: 4D-reconstruction of the Schwalbenberg loess-palaeosol-sequence (Middle Rhine Valley, Germany). *Catena* 196, 104913. doi:10.1016/j.catena.2020.104913

Fitzsimmons, K. E., Doboș, A., Probst, M., and Iovita, R. (2020). Thinking outside the box at open-air archeological contexts: examples from loess landscapes in southeast Romania. *Front. Earth Sci.* 8, 561207. doi:10.3389/feart.2020.561207

Fitzsimmons, K. E., Marković, S. B., and Hambach, U. (2012). Pleistocene environmental dynamics recorded in the loess of the middle and lower danube Basin. *Quat. Sci. Rev.* 41, 104–118. doi:10.1016/j.quascirev.2012.03.002

Fu, Q., Hajdinjak, M., Moldovan, O. T., Constantin, S., Mallick, S., Skoglund, P., et al. (2015). An early modern human from Romania with a recent Neanderthal ancestor. *Nature* 524, 216–219. doi:10.1038/nature14558

Fuchs, M., Rousseau, D.-D., Antoine, P., Hatté, C., Gauthier, C., Marković, S., et al. (2008). Chronology of the last climatic cycle (upper Pleistocene) of the surduk loess sequence, Vojvodina, Serbia. *Boreas* 37, 66–73. doi:10.1111/j.1502-3885.2007.00012.x

Gavrilov, N. B., Marković, S. B., Schaetzl, R. J., Tošić, I. A., Zeeden, C., Obreht, I., et al. (2018). Prevailing surface winds in Northern Serbia in the recent and past time periods; modern- and past dust deposition. *Aeolian Res.* 31, 117–129. doi:10.1016/j.aeolia.2017.07.008

Geological Institute of Serbia (2009). *Basic geological map of Serbia 1: 100000, Vršac Sheet number L34-103*. Belgrade: Faculty of Mining and Geology, University of Belgrade. Available at: http://geoliss.mre.gov.rs/OGK/RasterSrbija/.

Gerlach, R., Fischer, P., Meurers-Balke, J., Mirschenz, M., Röbke, A., Hadler, H., Willershäuser, T., and Vött, A. (2019). Römische Hafenstandorte: Standortbedingungen und Flussdynamik am niedergermanischen Rheinlimes von Königswinter bis Kleve-Rindern. Bonner Beiträge zur Vor- und Frühgeschichtlichen Archäologie, 22, 17–77.

Guérin, G., Frouin, M., Talamo, S., Aldeias, V., Bruxelles, L., Chiotti, L., et al. (2015). A multi-method luminescence dating of the Palaeolithic sequence of La Ferrassie based on new excavations adjacent to the La Ferrassie 1 and 2 skeletons. *J. Archaeol. Sci.* 58, 147–166.

Hauck, T. C., Lehmkuhl, F., Zeeden, C., Bösken, J., Thiemann, A., and Richter, J. (2018). The Aurignacian way of life: contextualizing early modern human adaptation in the Carpathian Basin. *Quat. Int.* 485, 150–166. doi:10.1016/j.quaint.2017.10.020

Hublin, J. J., Sirakov, N., Aldeias, V., Bailey, S., Bard, E., Delvigne, V., et al. (2020). Initial upper palaeolithic *Homo sapiens* from bacho kiro Cave, Bulgaria. *Nature* 581, 299–302. doi:10.1038/s41586-020-2259-z

Iovita, R., Doboș, A., Fitzsimmons, K. E., Probst, M., Hambach, U., Robu, M., et al. (2014). Geoarchaeological prospection in the loess steppe: preliminary results from the Lower danube survey for Paleolithic sites (LoDanS). *Quat. Int.* 351, 98–114. doi:10.1016/j.quaint.2013.05.018

ISO (2009). *Soil quality–Determination of particle size distribution in mineral soil material–Method by sieving and sedimentation*. Berlin: Beuth, 11277.

Kels, H., Protze, J., Sitlivy, V., Hilgers, A., Zander, A., Anghelinu, M., et al. (2014). Genesis of loess-like sediments and soils at the foothills of the Banat Mountains, Romania – examples from the paleolithic sites românești and coșava. *Quat. Int.* 351, 213–230. doi:10.1016/j.quaint.2014.04.063

Klasen, N., Kehl, M., Mikdad, A., Brückner, H., and Weniger, G.-C. (2018). Chronology and formation processes of the Middle to Upper Palaeolithic deposits of Ifri n'Ammar using multi-method luminescence dating and micromorphology. *Quat. Int.* 485, 89–102.

Kozłowski, J. (1992). The Balkans in the middle and upper palaeolithic: the gate to Europe or a cul-de-sac? *Proc. Prehist. Soc.* 58, 1–20.

Krézsek, C., and Olariu, C. (2020). Filling of sedimentary basins and the birth of large rivers: the lower danube network in the Dacian Basin, Romania. *Glob. Planet. Change* 197, 103391. doi:10.1016/j.gloplacha.2020.103391

Kulig, G. (2005). Erstellung einer Auswertesoftware zur altersbestimmung mittels Lumineszenzverfahren unter spezieller Berücksichtigung des Einflusses radioaktiver Ungleichgewichte in der 238-U-Zerfallsreihe. Bakkalaureusarbeit Network Computer TU Freib.

Mandić, M., and Borić, D. (2015). "Pećina kod trajanove table," in *In pećina kod trajanove table*. Editor J. Ćalić (Belgrade: Public Enterprise "Djerdap National Park), 84–89.

Marín-Arroyo, A. B., and Mihailović, B. (2017). The chronometric dating and subsistence of late Neanderthals and early anatomically modern humans in the central Balkans: insights from Šalitrena Pećina (Monica, Serbia). *J. Anthropol. Res.* 73, 413–447. doi:10.1086/693054

Marković, S. B., Sümegi, P., Stevens, T., Schaetzl, R. J., Obreht, I., Chu, W., et al. (2018). The Crvenka loess-paleosol sequence: a record of continuous grassland domination in the southern Carpathian Basin during the Late Pleistocene. *Palaeogeogr. Palaeoclimatol. Palaeoecol.* 509, 33–46. doi:10.1016/j.palaeo.2018.03.019

Marković, S. B., Timar-Gabor, A., Stevens, T., Hambach, U., Popov, D., Tomić, N., et al. (2014). Environmental dynamics and luminescence chronology from the Orlovat loess-Paleosol sequence (Vojvodina, Northern Serbia). *J. Quat. Sci.* 29, 189–199.

Marović, M., Toljić, M., Rundić, L., and Milivojević, J. (2007). *Neoalpine tectonics of Serbia*. Belgrade, Serbia: Serbian Geological Society.

Matenco, L., and Radivojević, D. (2012). On the formation and evolution of the Pannonian Basin: constraints derived from the structure of the junction area between the Carpathians and Dinarides. *Tectonics* 31, 1–31. doi:10.1029/2012TC003206

Mihailović, D. (1992). *Aurignacian flint industry from the site Crvenka-At near Vršac*. Belgrade: Centre for Archaeological Research: Faculty of Philosophy in Belgrade.

Mihailović, D., Mihailović, B., and Lopičić, M. (2011). "The palaeolithic in northern Serbia," in *The prehistory of Banat: the palaeolithic and mesolithic*. Editors N. Tasić, F. Drașovean, and B. Jovanović (Bucharest: Publishing House of the Romanian Academy), 77–93.

Mihailović, D. (2020). Push-and-pull factors of the middle to upper paleolithic transition in the Balkans. *Quat. Int.* 551, 47–62. doi:10.1016/j.quaint.2019.10.010

Miller, R. (2014). "Maisières-Canal: an open-air Aurignacian workshop" in *Encyclopedia of global Archaeology*. Editor C. Smith (New York, NY: Springer) doi:10.1007/978-1-4419-0465-2_1986

Müller, I. (1769). Mappa geographica novissima regni hungariae. Available at: https://maps.hungaricana.hu/hu/MOLTerkeptar/11272/view/?pg=6&bbox=4590%2C-3664%2C8209%2C-1572 (Accessed October 24, 2019).

Murray, A. S., Thomsen, K. J., Masuda, N., Buylaert, J. P., and Jain, M. (2012). Identifying well-bleached quartz using the different bleaching rates of quartz and feldspar luminescence signals. *Radiat. Meas.* 47 (9), 688–695. doi:10.1016/j.radmeas.2012.05.006

Murray, A. S., and Wintle, A. G. (2000). Luminescence dating of quartz using an improved single-aliquot regenerative-dose protocol. *Radiat. Meas.* 32, 57–73. doi:10.1016/S1350-4487(99)00253-X

Murray, A. S., and Wintle, A. G. (2003). The single aliquot regenerative dose protocol: potential for improvements in reliability. *Radiat. Meas.* 37, 377–381. doi:10.1016/S1350-4487(03)00053-2

Nelson, M. S., Gray, H. J., Johnson, J. A., Rittenour, T. M., Feathers, J. K., and Mahan, S. A. (2015). User guide for luminescence sampling in archaeological and geological contexts. *Adv. Archaeol. Pract.* 3, 166–177. doi:10.7183/2326-3768.3.2.166

Nelson, M. S., and Rittenour, T. M. (2015). Using grain-size characteristics to model soil water content: application to dose-rate calculation for luminescence dating. *Radiat. Meas.* 81, 142–149. doi:10.1016/j.radmeas.2015.02.016

Nottebaum, V., Stauch, G., Hartmann, K., Zhang, J., and Lehmkuhl, F. (2015). Unmixed loess grain size populations along the northern Qiqian Shan (China): relationships between geomorphologic, sedimentologic and climatic controls. *Quat. Int.* 372, 151–166. doi:10.1016/j.quaint.2014.12.071

Obreht, I., Hambach, U., Veres, D., Zeeden, C., Bösken, J., Stevens, T., et al. (2017). Shift of large-scale atmospheric systems over Europe during late MIS 3 and implications for modern human dispersal. *Sci. Rep.* 7, 5848. doi:10.1038/s41598-017-06285-x

Obreht, I., Zeeden, C., Hambach, U., Veres, D., Marković, S. B., and Lehmkuhl, F. (2019). A critical reevaluation of palaeoclimatic proxy records from loess in the Carpathian Basin. *Earth-Sci. Rev.* 190, 498–520. doi:10.1016/j.earscirev.2019.01.020

Obreht, I., Zeeden, C., Schulte, P., Hambach, U., Eckmeier, E., Timar-Gabor, A., et al. (2015). Aeolian dynamics at the Orlovat loess–paleosol sequence, northern Serbia, based on detailed textural and geochemical evidence. *Aeolian Res.* 18, 69–81. doi:10.1016/j.aeolia.2015.06.004

Özer, M., Orhan, M., and Işik, N. S. (2010). Effect of particle optical properties on size distribution of soils obtained by laser diffraction. *Environ. Eng. Geosci.* 16, 163–173. doi:10.2113/gseegeosci.16.2.163

Perić, Z., Adophi, E. L., Buylaert, J. P., Stevens, T., Újvári, G., Marković, S. B., et al. (2019). Quartz OSL dating of late Quaternary Chinese and Serbian loess: a cross Eurasian comparison of dust and mass accumulation rates. *Quat. Int.* 509A, 30–44. doi:10.1016/j.quaint.2018.01.010

Perić, Z., Marković, S. B., Sipos, Gy., Gavrilov, M. B., Thiel, C., Zeeden, C., et al. (2020). A post-IR IRSL chronology and dust mass accumulation rates of the Novak loess-paleosol sequence in northeastern Serbia. *Boreas* 49, 841–857. doi:10.1111/bor.12459

Popov, D., Vandenberghe, D. A. G., and Marković, S. B. (2012). Luminescence dating of fluvial deposits in Vojvodina, N Serbia: first results. *Quat. Geochronol.* 13, 42–51. doi:10.1016/j.quageo.2012.08.002

Pötter, S., Schmitz, A., Lücke, A., Schulte, P., Obreht, I., Zech, M., et al. (2021). Middle to Late Pleistocene environments based on stableorganic carbon and nitrogen isotopes of loess-palaeosol sequences from the Carpathian Basin. *Boreas* 50, 184–204. doi:10.1111/bor.12470

Păunescu, A. (2001). *Paleoliticul și mezoliticul din spațiul transiliac*. Bucharest: Agir.

R Core Team (2020). *R: a language and environment for statistical computing*. Available at: http://www.R-project.org/. Date of access: 2020/12/08.

Radovanović, I. (1986). Vršac-At, palaeolitsko nalazište. *Arheol. Pregl.* 25, 11–12.

Richards, M. P., and Trinkaus, E. (2009). Out of Africa: modern human origins special feature: isotopic evidence for the diets of European Neanderthals and early modern humans. *Proc. Natl. Acad. Sci. U.S.A.* 106, 16034–16039. doi:10.1073/pnas.0903821106

Rundić, L., Ganic, M., Knezevic, S., Radivojevic, D., and Radonjic, M. (2019). Stratigraphic implications of the mio-pliocene geodynamics in the area of Mt. Avala: new evidence from torlak hill and beli potok (Belgrade, Serbia). *Geol. Croat.* 72, 109–128. doi:10.4154/gc.2019.11

Schmidt, C., Sitlivy, V., Anghelinu, M., Chabai, V., Kels, H., Uthmeier, T., et al. (2013). First chronometric dates (TL and OSL) for the Aurignacian open-air site of Românești-Dumbrăvița I, Romania. *J. Archaeol. Sci.* 40, 3740–3753. doi:10.1016/j.jas.2013.04.003

Schmidt, E. D., Machalett, B., Marković, S. B., Tsukamoto, S., and Frechen, M. (2010). Luminescence chronology of the upper part of the Stari Slankamen loess sequence (Vojvodina, Serbia). *Quat. Geochronol.* 5, 137–142. doi:10.1016/j.quageo.2009.09.006

Schulte, P., Lehmkuhl, F., Kels, H., Loibl, C., Klasen, N., and Hauck, T. (2014). Environmental change indicated by grain-size variations and trace elements: examples from two different sections - the sandy-loess sediments from the Doroshivtsy site (Ukraine) and the loess section Semlac (Romania). *Proscience* 1, 106–112. doi:10.14644/dust.2014.017

Schulte, P., Lehmkuhl, F., Steininger, F., Loibl, D., Lockot, G., Protze, J., et al. (2016). Influence of HCl pretreatment and organo-mineral complexes on laser diffraction measurement of loess–paleosol-sequences. *Catena* 137, 392–405. doi:10.1016/j.catena.2015.10.015

Schwarz, U. (2014). "Hydromorphology of the danube," in *The danube river basin* (Berlin, Heidelberg: Springer), 469–479.

Sitlivy, V., Chabai, V., Anghelinu, M., Uthmeier, T., Kels, H., Hilgers, A., et al. (2012). The earliest Aurignacian in Romania: new investigations at the open air site of Românești-Dumbrăvița I (Banat). *Quartär* 59, 85–130.

Sitlivy, V., Nită, L., Băltean, I., Anghelinu, M., Uthmeier, T., Hilger, A., et al. (2014). "Placing the aurignacian from Banat (southwestern Romania) into the European early upper paleolithic context," in *Modes de Contactes et de Deplacements au Paléolithique Eurasiatique*. Editors M. Otte and F. le (Brun-Ricalens Liége: ERAUL), 243–277.

Soficaru, A., Dobos, A., and Trinkaus, E. (2006). Early modern humans from the pestera Muierii, baia de Fier, Romania. *Proc. Natl. Acad. Sci. U.S.A.* 103, 17196–17201. doi:10.1073/pnas.0608443103

Soficaru, A., Petrea, C., Doboș, A., and Trinkaus, E. (2007). The human cranium from the Peștera Cioclovina uscată, Romania. *Curr. Anthropol.* 48, 611–619. doi:10.1086/519915

Sprafke, T. (2016). *Löss in Niederösterreich – archiv quartärer Klima- und Landschaftsveränderungen (Loess in Lower Austria - archive of Quaternary climate and landscape development)*. Würzburg: Würzburg University Press.

Starkel, L., Michczunska, D. J., Gebica, P., Kiss, T., Panin, A., and Persoiu, I. (2015). Climatic fluctuations reflected in the evolution of fluvial systems of Central-Eastern Europe (60-80 ka cal BP). *Quat. Int.* 388, 97–118. doi:10.1016/j.quaint.2015.04.017

Staubwasser, M., Drăgușin, V., Onac, B. P., Assonov, S., Ersek, V., Hoffmann, D. L., et al. (2018). Impact of climate change on the transition of Neanderthals to modern humans in Europe. *Proc. Natl. Acad. Sci. U.S.A.* 115, 9116. doi:10.1073/pnas.1808647115

Sušić, Z., Toljić, M., Bulatović, V., Ninkov, T., and Stojadinović, U. (2016). Present-day horizontal mobility in the Serbian part of the Pannonian Basin; inferences from the geometric analysis of deformations. *Acta Geophys.* 64, 1626–1654. doi:10.1515/acgeo-2016-0074

Teyssandier, N., and Zilhão, J. (2018). On the entity and antiquity of the Aurignacian at Willendorf (Austria): implications for modern human emergence in Europe. *J. Paleolit. Archaeol.* 1, 107–138. doi:10.1007/s41982-017-0004-4

Thiel, C., Buylaert, J.-P., Murray, A., Terhorst, B., Hofer, I., Tsukamoto, S., et al. (2011). Luminescence dating of the Stratzing loess profile (Austria) – testing the potential of an elevated temperature post-IR IRSL protocol. *Quat. Int.* 234, 23–31. doi:10.1016/j.quaint.2010.05.018

Thomsen, K. J., Murray, A. S., Jain, M., and Bøtter-Jensen, L. (2008). Laboratory fading rates of various luminescence signals from feldspar-rich sediment extracts. *Radiat. Meas.* 43 (9), 1474–1486. doi:10.1016/j.radmeas.2008.06.002

Tikhonov, A. (2008). The IUCN red list of threatened species 2008: e.T136721A4332142. *Bos Primigenius*, 7 doi:10.2305/IUCN.UK.2008.RLTS.T136721A4332142.en

Timár, G., Székely, B., Molnár, G., Ferencz, C., Kern, A., Galambos, C., et al. (2008). Combination of historical maps and satellite images of the Banat region—re-appearance of an old wetland area. *Glob. Planet. Change* 62, 29–38. doi:10.1016/j.gloplacha.2007.11.002

Toljić, M., Matenco, L., Ducea, M. N., Stojadinović, U., Milivojević, J., and Đerić, N. (2013). The evolution of a key segment in the Europe–Adria collision: the Fruška Gora of northern Serbia. *Glob. Planet Change* 103, 39–62. doi:10.1016/j.gloplacha.2012.10.009

Tourloukis, V. (2016). "On the spatio-temporal distribution of mediterranean lower paleolithic sites: a geoarchaeological perspective," in *Paleoanthropology of the Balkans and anatolia: human evolution and its context*. Editors K. Harvati and M. Roksandic (Dordrecht: Springer), 303–323.

Trinkaus, E., Milota, S., Rodrigo, R., Mircea, G., and Moldovan, O. (2003a). Early modern human cranial remains from the Peştera cu Oase, Romania. *J. Hum. Evol.* 45, 245–253. doi:10.1016/j.jhevol.2003.08.003

Trinkaus, E., Moldovan, O., Milota, S., Bîlgăr, A., Sarcina, L., Athreya, S., et al. (2003b). An early modern human from the Peştera cu Oase, Romania. *Proc. Natl. Acad. Sci. U.S.A.* 100, 11231–11236. doi:10.1073/pnas.2035108100

Trinkaus, E., Constantin, S., and Zilhão, J. (2012). *Life and death at the Peştera cu Oase: a setting for modern human emergence in Europe*. New York: Oxford University Press.

Trinkaus, E., Soficaru, A., Doboș, A., Constantin, S., Zilhão, J., and Richards, M. (2009). Stable isotope evidence for early modern human diet in southeastern Europe: peştera cu Oase, Peştera muierii and peştera cioclovina uscată. *Mater. Cercetări Arheolog.* 5, 4–14.

Vandenberghe, J., Kasse, C., Popov, D., Markovic, S. B., Vandenberghe, D., Bohncke, S., et al. (2018). Specifying the external impact on fluvial lowland evolution: the Last Glacial Tisza (Tisa) catchment in Hungary and Serbia. *Quaternary* 1, 14. doi:10.3390/quat1020014

Vasiliniuc, Ş., Vandenberghe, D. A. G., Timar-Gabor, A., Panaiotu, C., Cosma, C., and van den Haute, P. (2012). Testing the potential of elevated temperature post-IR IRSL signals for dating Romanian loess. *Quat. Geochronol.* 10, 75–80. doi:10.1016/j.quageo.2012.02.014

Vlaminck, S., Kehl, M., Lauer, T., Shahriari, A., Sharifi, J., Eckmeier, E., et al. (2016). Loess-soil sequence at toshan (northern Iran): insights into late Pleistocene climate change. *Quat. Int.* 399, 122–135. doi:10.1016/j.quaint.2015.04.028

Weninger, B., Joris, O., and Danzeglocke, U. (2008). *CalPal-2007. Cologne, radiocarbon calibration & palaeoclimate research package*. Available at: http://www.calpal.de.

Xiao, J., Chang, Z., Fan, J., Zhou, L., Zhai, D., Wen, R., et al. (2012). The link between grain-size components and depositional processes in a modern clastic lake: grain-size components of Hulun Lake sediments. *Sedimentology* 59, 1050–1062. doi:10.1111/j.1365-3091.2011.01294.x

Zeeden, C., Dietze, M., and Kreutzer, S. (2018). Discriminating luminescence age uncertainty composition for a robust Bayesian modelling. *Quat. Geochron.* 43, 30–39. doi:10.1016/j.quageo.2017.10.001

Zeeden, C., Hambach, U., Klasen, N., Fischer, P., Schulte, P., Nett, J. J., et al. (2021). Sedimentology of a late Quaternary lacustrine record from the south-eastern Carpathian Basin. *J. Quat. Sci.*

Zeeden, C., Kels, H., Hambach, U., Schulte, P., Protze, J., Eckmeier, E., et al. (2016). Three climatic cycles recorded in a loess-paleosol sequence at Semlac (Romania) – implications for dust accumulation in south-eastern Europe. *Quat. Sci. Rev.* 154, 130–142. doi:10.1016/j.quascirev.2016.11.002

Zeeden, C., Krauß, L., Kels, H., and Lehmkuhl, F. (2017). Digital image analysis of outcropping sediments: comparison to photospectrometric data from quaternary loess deposits at Șanovița (Romania) and Achenheim (France). *Quat. Int.* 429, 100–107. doi:10.1016/j.quaint.2016.02.047

Zilhão, J., Trinkaus, E., Constantin, S., Milota, S., Gherase, M., Sarcina, L., et al. (2007). "The Peştera cu Oase people, Europe's earliest modern humans," in *Rethinking the human revolution: new behavioural and biological perspectives on the origin and dispersal of modern humans*. Editors P. Mellars, K. Boyle, O. Bar-Yosef, and C. Stringer (Cambridge, UK: McDonald Institute for Archaeological Research), 249–262.

Conflict of Interest: The authors declare that the research was conducted in the absence of any commercial or financial relationships that could be construed as a potential conflict of interest.